


# Exciton binding energy and screening length in two-dimensional semiconductors

Hieu T. Nguyen-Truong \*

*Laboratory of Applied Physics, Science and Technology Advanced Institute, Van Lang University, Ho Chi Minh City, Vietnam  
and Faculty of Technology, Van Lang University, Ho Chi Minh City, Vietnam*



(Received 1 February 2022; revised 9 April 2022; accepted 19 May 2022; published 31 May 2022)

We approximately solve the Schrödinger equation for two-dimensional Wannier-Mott excitons in the effective-mass approximation and derive an expression for the exciton energy levels, hence the exciton binding energy. The electron-hole interaction is described by the Rytova-Keldysh potential in a logarithmic approximation. From the derived expression, we introduce approximate expressions to experimentally determine the exciton binding energy (along with the quasiparticle band gap), the screening length, and the exciton reduced mass from measured exciton transition energies of the ground state (1s), and the first (2s) and the second (3s) excited states. Our results agree well with experimental data and theoretical calculations.

DOI: [10.1103/PhysRevB.105.L201407](https://doi.org/10.1103/PhysRevB.105.L201407)

An exciton is an electron-hole pair bound by Coulomb interactions in semiconductors. In two-dimensional (2D) semiconductors, the Coulomb interaction is significantly enhanced due to the effects of spatial quantum confinement and reduced dielectric screening [1]. As a consequence, the electron-hole pairs are tightly bound, and the exciton states are stable even at room temperature [2–6]. These tightly bound excitons may have binding energies up to hundreds of meV and dominate the optical response. In particular, a quantitative understanding of *s*-state excitons and the ground-state (1s) exciton binding energy is important for optoelectronic applications [7–9].

In the Wannier-Mott exciton model [10,11] for three-dimensional (3D) semiconductors, an electron-hole pair in parabolic bands is treated as a hydrogen atom, where the hole plays the role of the proton, and the electron-hole interaction is described by the Coulomb potential [12]. The analytical solution of the Schrödinger equation for the hydrogen problem has been well known. The 3D hydrogenic exciton binding energy (in Hartree atomic units,  $\hbar = m_0 = e = 1$ ) is  $E_b^{3D} = \mu/(2\varepsilon_0^2)$ , where  $\varepsilon_0$  is the background dielectric constant, and  $\mu$  is the exciton reduced mass. The 2D hydrogenic exciton energy levels [13] are  $E_n^{2D} = -\mu/[2\varepsilon_0^2(n - 1/2)^2]$ , where  $n = 1, 2, 3, \dots$  is the principal quantum number. Then, the 2D hydrogenic exciton binding energy is  $E_b^{2D} = -E_1^{2D} = 4E_b^{3D}$ . However, the exciton binding energy in 2D semiconductors has been shown to deviate significantly from the hydrogenic model due to the nonlocal screening of electron-hole Coulomb interactions [2,3,6,14,15]. The 2D excitons of the lowest-lying states are nonhydrogenic, though the ones of the higher-lying states exhibit hydrogenic behaviors.

The 2D exciton in a monolayer semiconductor is usually modeled as an electron-hole pair in the plane of a dielectric layer of zero thickness. The electron-hole interaction potential  $V$  in momentum space ( $q$ ) is found by solving the Poisson equation  $V(q) = -2\pi/[q(\kappa + r_0q)]$ , where  $\kappa$  is the average

dielectric constant of the surrounding environment, and the screening length  $r_0 = 2\pi\alpha$  with  $\alpha$  being the 2D polarizability of the material [16]. The inverse Fourier transform of  $V(q)$  is known as the Rytova-Keldysh (RK) potential in real space [17,18],

$$V(r) = -\frac{\pi}{2r_0} \left[ H_0\left(\frac{\kappa r}{r_0}\right) - Y_0\left(\frac{\kappa r}{r_0}\right) \right], \quad (1)$$

where  $H_0$  is the Struve function,  $Y_0$  is the Neumann function (also called the Bessel function of the second kind), and  $r$  is the electron-hole distance.

Analytically solving the Schrödinger equation for the RK potential requires approximations. This potential is often approximated by the Coulomb potential  $-1/(\kappa r)$ , and recently by the Kratzer potential  $-1/(\kappa r) + g^2 r_0/(\kappa r)^2$  with  $g$  being an adjustable parameter [19]. The RK potential behaves as a Coulomb potential at large distances, but diverges logarithmically at short ones. Neglecting this logarithmic divergence may lead to unreliable results for the ground-state exciton due to its nonhydrogenic nature. A complete analytical solution of the Schrödinger equation for a logarithmic potential is lacking. Nonetheless, asymptotic solutions for this problem have been reported in literature [20–23].

Here, using the logarithmic approximation

$$V(r) \approx -\frac{1}{r_0} \ln \left( 1 + \frac{r_0}{\kappa r} \right), \quad (2)$$

which satisfies both limits of the RK potential  $V(r) \approx -1/(\kappa r)$  for  $\kappa r \gg r_0$  and  $V(r) \sim \ln(\kappa r/r_0)$  for  $\kappa r \ll r_0$ , we approximately solve the Schrödinger equation for 2D Wannier-Mott excitons in the effective-mass approximation  $(-\frac{1}{2\mu}\nabla^2 + V)\psi = E\psi$ . The envelope function  $\psi$  in polar coordinates ( $r, \varphi$ ) has the form  $\psi(r, \varphi) = \frac{1}{\sqrt{2\pi}} e^{im\varphi} R(r)$ , where  $R(r)$  is the solution of the radial equation  $r^2 R'' + rR' + [2\mu(E - V)r^2 - m^2]R = 0$ , and  $m = 0, \pm 1, \pm 2, \dots$  is the angular quantum number. For *s*-state excitons ( $m = 0$ ), we

\*nguyentruongthanhhieu@vlu.edu.vn

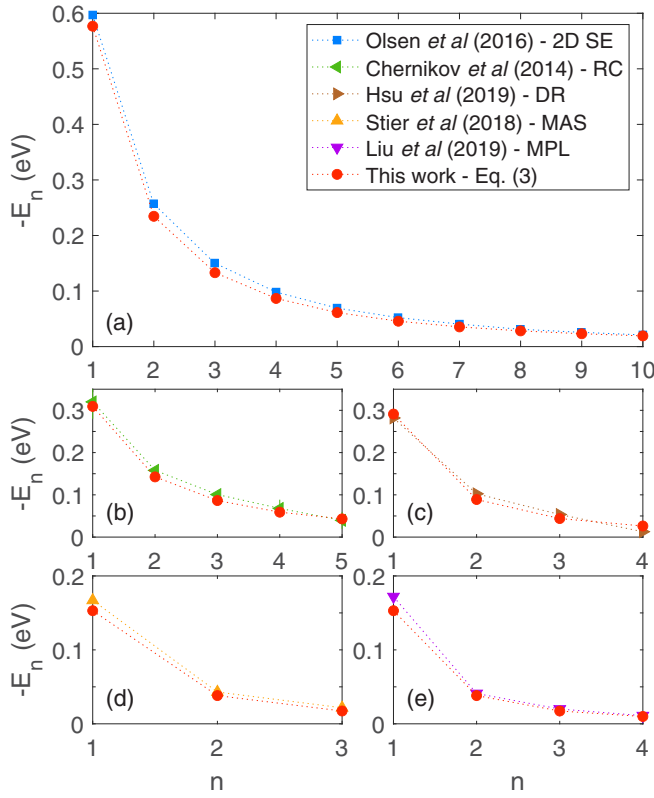


FIG. 1. The  $ns$ -state exciton energy levels: red symbols—this work; blue symbols—numerical solution of the 2D Schrödinger equation (SE) for an isolated monolayer  $2H$ -WS<sub>2</sub> [14]; green symbols—experimental data from measurements of reflectance contrast (RC) spectra for a monolayer WS<sub>2</sub> on a SiO<sub>2</sub>/Si substrate (a 300-nm SiO<sub>2</sub> layer on a Si substrate) [2]; brown symbols—experimental data from measurements of differential reflectance (DR) spectra for a monolayer WS<sub>2</sub> on a sapphire substrate [30]; orange and violet symbols—experimental data from measurements of magnetoabsorption spectroscopy (MAS) [7] and of magnetophotoluminescence (MPL) [31] for a monolayer WSe<sub>2</sub> encapsulated by hexagonal boron nitride, respectively.

find

$$E_n = -\frac{25\kappa^2}{8\mu r_0^2} \left( \sqrt{n - \frac{1}{2}} + 2\sqrt{\frac{2\mu r_0}{5\kappa^2}} - \sqrt{n - \frac{1}{2}} \right)^4. \quad (3)$$

To derive this expression, besides the approximation (2), we also use other approximations which are valid for large  $r$ . We present the mathematical derivation in the Supplemental Material [24] (see also Refs. [25–29] therein). In the following, we compare our results with experimental data and theoretical calculations, including those based on the Bethe-Salpeter equation (BSE).

Figure 1 depicts the  $ns$ -state exciton energy levels for 2D semiconductors WS<sub>2</sub> and WSe<sub>2</sub>. In Fig. 1(a), our results are consistent with the numerical solutions of the 2D Schrödinger equation [14] for an isolated monolayer  $2H$ -WS<sub>2</sub> ( $\kappa = 1$ ,  $\mu = 0.19$ ,  $\alpha = 5.25$  Å [14],  $r_0 = 2\pi\alpha \approx 32.99$  Å). In experiments, a monolayer semiconductor is usually placed on an insulating substrate or sandwiched between two dielectric layers. Then,

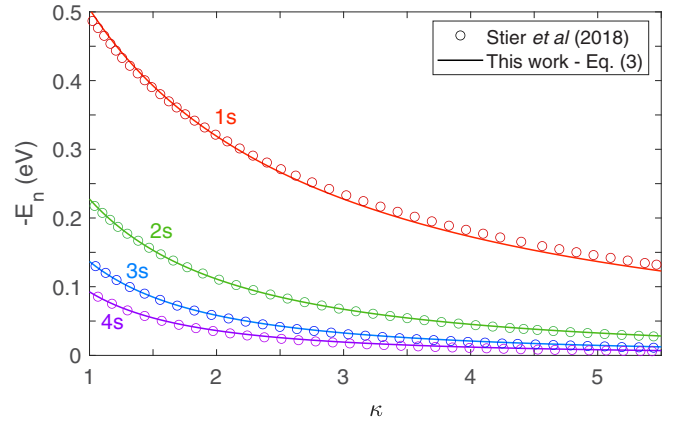


FIG. 2. The hBN-encapsulated monolayer WSe<sub>2</sub>: the  $ns$ -state exciton energy levels vs the average dielectric constant.

the influence of the surrounding dielectric environment should be taken into account.

For a 2D semiconductor placed on an insulating substrate, the average dielectric constant of the surrounding environment (substrate and vacuum)  $\kappa = (1 + \epsilon_{\text{sub}})/2$ , where  $\epsilon_{\text{sub}}$  is the dielectric constant of the substrate. In Figs. 1(b) and 1(c), our results agree with experimental data from measurements of reflectance contrast spectra [2,30] for a monolayer WS<sub>2</sub> ( $r_0 = 37.89$  Å,  $\mu = 0.167$  [29]) on a SiO<sub>2</sub>/Si substrate ( $\kappa = 2$  [32]) and on a sapphire substrate ( $\kappa = 2.07$  [30]), respectively.

For a 2D semiconductor sandwiched between two dielectric layers,  $\kappa = (\epsilon_1 + \epsilon_2)/2$ , where  $\epsilon_1$  and  $\epsilon_2$  are the dielectric constants of the two layers. In Figs. 1(d) and 1(e), our results are consistent with experimental data from measurements of magnetoabsorption spectroscopy [7] and of magnetophotoluminescence [31] for a monolayer WSe<sub>2</sub> ( $r_0 = 45$  Å [7],  $\mu = 0.25$ ) encapsulated by hexagonal boron nitride (hBN,  $\epsilon_{\text{hBN}} = 4.5$  [29],  $\kappa = 4.5$ ).

Figure 2 displays the exciton energy levels  $E_n$  as functions of  $\kappa$ . Our results agree with the numerical calculations for a hBN-encapsulated monolayer WSe<sub>2</sub> [7]. The separations between energy levels reduce with increasing  $\kappa$ . In the limit of large  $\kappa$ , the energy separations  $\Delta_{1n}$  between the ground state (1s) and the  $ns$  excited states approach the exciton binding energy  $E_b = -E_1$ . In the 2D hydrogenic model,  $E_b^{\text{2D}} = \frac{9}{8}\Delta_{12}$ . However, this relation is less reliable for nonhydrogenic excitons [3]. A relation between the exciton binding energy  $E_b$  and the energy separations  $\Delta_{12}$ ,  $\Delta_{13}$  is introduced later.

Figure 3 shows a comparison of exciton binding energies between our results and BSE values from the Computational 2D Materials Database (C2DB) [25,26] for 58 isolated monolayer semiconductors (see Supplemental Material for details). Our results agree reasonably with the BSE values; in most cases the absolute error  $|E_b - E_b^{\text{BSE}}|$  is less than 0.05 eV (symbols within the gray region). In general, the exciton binding energy tends to increase with increasing quasiparticle band gap (indicated by the symbol color). Both the exciton binding energy and quasiparticle band gap tend to decrease with increasing screening length. In the limit of large  $\mu r_0/\kappa^2$ , the exciton binding energy is inversely proportional to the screening length:  $E_b \approx 5/r_0$ . In such a limit, e.g., for a sufficient large screening length, the exciton binding energy is

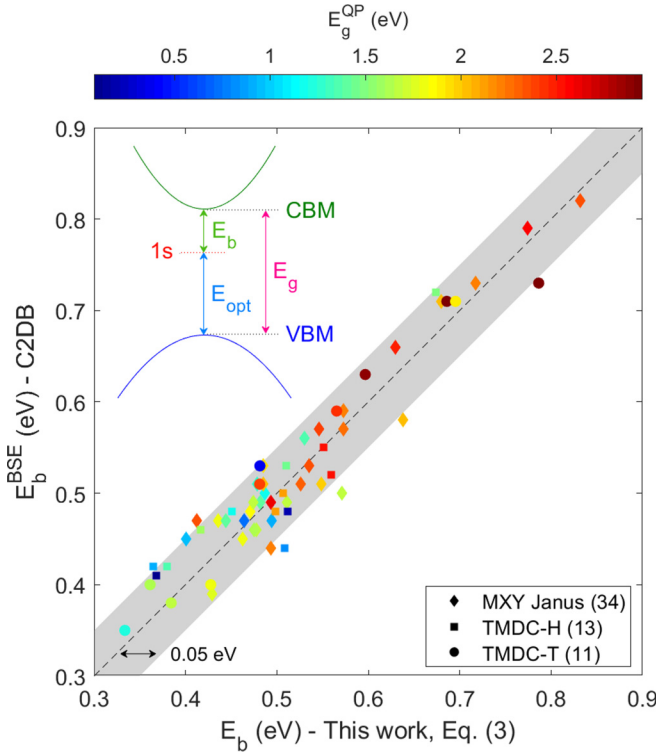


FIG. 3. The exciton binding energy for 58 isolated monolayer semiconductors (34 MX2 Janus, 13 TMDC-H, and 11 TMDC-T). The symbol color indicates the quasiparticle band gap. Data are taken from the Computational 2D Materials Database (C2DB) [25,26]. The inset shows an illustration of the band structure.

almost mass and dielectric independent, and the screening length plays a decisive role in determining the exciton binding energy.

In addition to comparing with the BSE calculations, we also compare with variational and Monte Carlo calculations. Table I lists the exciton binding energy for monolayer semiconductors  $MX_2$  ( $M = \text{Mo}, \text{W}; X = \text{S}, \text{Se}$ ). The materials are isolated ( $\kappa = 1$ ) or placed on a silica substrate ( $\kappa = 2$  [32]), and the material parameters are taken from Ref. [29]. Our results agree well with those calculated by the variational method (VM) [33], the simplified variational method (simVM) [29], the stochastic variational method (stoVM) [34], the path integral Monte Carlo (PIMC) method [32], and the diffusion Monte Carlo (DMC) method [35]. Comparing to the freestanding case, the exciton binding energy for a monolayer semiconductor placed on a dielectric substrate is lower due to substrate effects. Under the influence of the surrounding dielectric environment, the strength of electron-hole interactions is decreased with increasing  $\kappa$ . As a result, the exciton binding energy is reduced, leading to a reduction of the quasiparticle band gap. The ability to tune the quasiparticle band gap (and the exciton binding energy) of 2D semiconductors by engineering the surrounding dielectric environment may be useful in nanotechnology [36].

Next, we introduce approximate expressions based on the expression (3) and the C2DB (see also Fig. 4),

$$\frac{E_b}{\Delta_{12}} \approx 1 + \frac{1}{3} \left( \frac{\mu r_0}{\kappa^2} \right)^{0.3}, \quad (4)$$

TABLE I. The exciton binding energy for monolayer semiconductors (isolated or placed on a silica substrate).

Material	Substrate	$E_b$ (eV)	Method	Ref.
MoS <sub>2</sub>	Isolated	0.5352		This work
		0.5557	simVM	[29]
		0.5550	stoVM	[34]
		0.5265(2)	PIMC	[32]
		0.5514	DMC	[35]
		0.54	VM	[33]
	Silica	0.3362		This work
		0.3486(2)	PIMC	[32]
MoSe <sub>2</sub>	Isolated	0.4720		This work
		0.4867	simVM	[29]
		0.4804	stoVM	[34]
		0.4769(2)	PIMC	[32]
		0.4778	DMC	[35]
		0.47	VM	[33]
	Silica	0.3069		This work
		0.2914	simVM	[29]
0.3229(2)		PIMC	[32]	
WS <sub>2</sub>	Isolated	0.5038		This work
		0.5301	simVM	[29]
		0.5235	stoVM	[34]
		0.5098(2)	PIMC	[32]
		0.5191	DMC	[35]
		0.50	VM	[33]
	Silica	0.3000		This work
		0.2892	simVM	[29]
0.3229(2)		PIMC	[32]	
WSe <sub>2</sub>	Isolated	0.4532		This work
		0.4738	simVM	[29]
		0.4702	stoVM	[34]
		0.4564(2)	PIMC	[32]
		0.4667	DMC	[35]
		0.45	VM	[33]
	Silica	0.2764		This work
		0.2652	simVM	[29]
0.2946(2)		PIMC	[32]	

and

$$\frac{\Delta_{13}}{\Delta_{12}} \approx 1.175 \left( \frac{\mu r_0}{\kappa^2} \right)^{0.04}, \quad (5)$$

where  $\Delta_{12}$ ,  $\Delta_{13}$  are the energy separations between the ground state and the first/second excited state. Consequently,

$$E_b \approx \Delta_{12} \left[ 1 + \frac{1}{3} \left( \frac{1}{1.175} \frac{\Delta_{13}}{\Delta_{12}} \right)^{7.5} \right]. \quad (6)$$

By definition, the quasiparticle band gap  $E_g$  is the sum of the exciton binding energy  $E_b$  and the optical gap  $E_{\text{opt}}$  (i.e., the lowest exciton transition energy). Therefore, we are able to determine both the exciton binding energy and the quasiparticle band gap by measuring exciton transition energies of the ground state ( $1s$ ), and the first ( $2s$ ) and the second ( $3s$ ) excited states, hence the energy separations  $\Delta_{12}$  and  $\Delta_{13}$ .

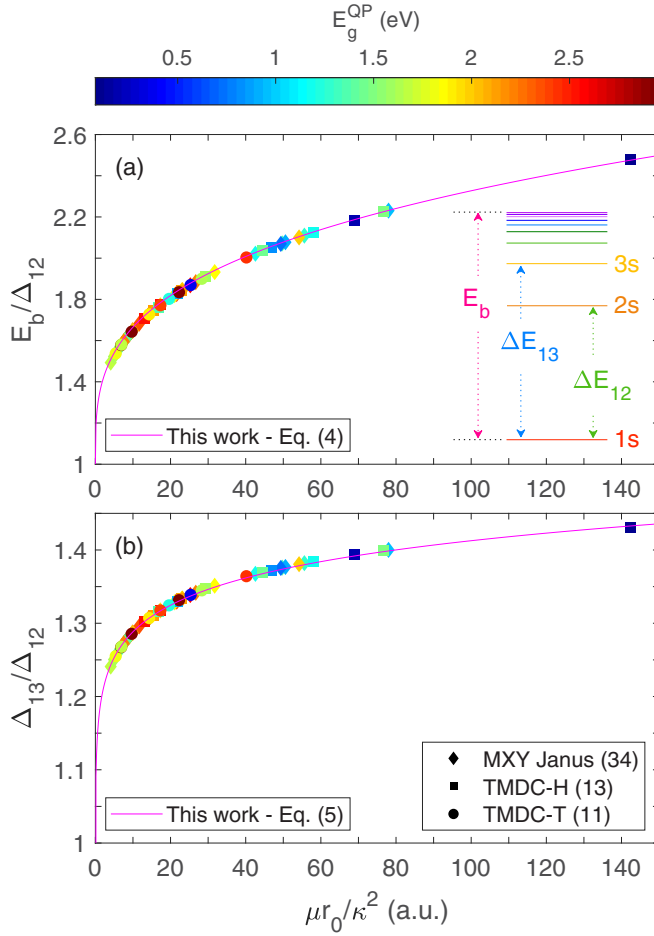


FIG. 4. The ratios (a)  $E_b/\Delta_{12}$  and (b)  $\Delta_{13}/\Delta_{12}$  as functions of  $\mu r_0/\kappa^2$  (in Hartree atomic units, a.u.). The symbol color indicates the quasiparticle band gap. The inset shows an illustration of  $ns$ -state exciton energy levels.

For example, from measurements of reflectance contrast (RC) spectra for a monolayer  $\text{WS}_2$  [2],  $E_{\text{opt}} = 2.09$  eV,  $\Delta_{12} = 0.163$  eV, and  $\Delta_{13} = 0.220$  eV, we obtain  $E_b = 0.316$  eV and  $E_g = 2.406$  eV. Our results are consistent with the RC data [2]:  $E_b = 0.32 \pm 0.04$  eV and  $E_g = 2.41 \pm 0.04$  eV. From measurements of differential reflectance (DR) spectra for a monolayer  $\text{WS}_2$  [30],  $E_{\text{opt}} = 2.017$  eV,  $\Delta_{12} = 0.180$  eV, and  $\Delta_{13} = 0.229$  eV, we obtain  $E_b = 0.289$  eV and  $E_g = 2.305$  eV. Our results agree with the DR data [30]:  $E_b = 0.282$  eV and  $E_g = 2.3$  eV. From measurements of photoluminescence excitation (PLE) spectroscopy for a monolayer  $\text{WS}_2$  [6],  $E_{\text{opt}} = 2.008$  eV,  $\Delta_{12} = 0.163$  eV, and  $\Delta_{13} = 0.227$  eV, we obtain  $E_b = 0.360$  eV and  $E_g = 2.368$  eV. Our results are close to the PLE data [6]:  $E_b = 0.32 \pm 0.05$  eV and  $E_g = 2.33 \pm 0.05$  eV. From measurements of two-photon photoluminescence (2PPL) excitation spectroscopy for a monolayer  $\text{WSe}_2$  [3],  $E_{\text{opt}} = 1.65$  eV,  $\Delta_{12} = 0.165$  eV, and  $\Delta_{13} = 0.231$  eV, we obtain  $E_b = 0.370$  eV and  $E_g = 2.020$  eV. Our results are consistent with the 2PPL data [3],  $E_b = 0.37$  eV and  $E_g = 2.02$  eV, which are independent of any exciton model. From measurements of polarized magnetooptical spectroscopy (PMS) for a monolayer  $\text{WSe}_2$  [7],  $E_{\text{opt}} = 1.723$  eV,  $\Delta_{12} = 0.124$  eV, and  $\Delta_{13} = 0.145$  eV, we obtain

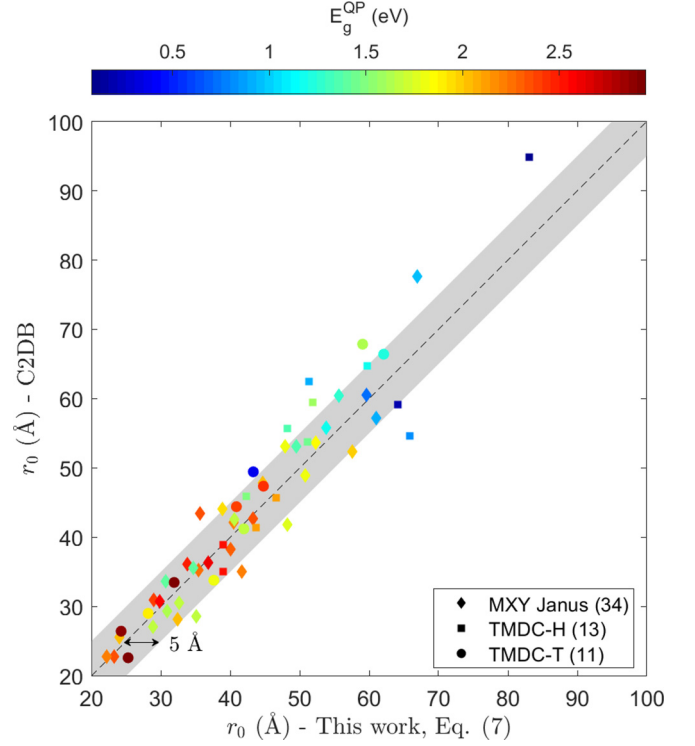


FIG. 5. Same as Fig. 3 but for the screening length.

$E_b = 0.165$  eV and  $E_g = 1.888$  eV. Our results agree with the PMS data [7]:  $E_b = 0.167$  eV and  $E_g = 1.89$  eV.

Apart from the exciton binding energy, we are also interested in the screening length. From the expression (3), we deduce the screening length as a function of the exciton binding energy,

$$r_0 = \frac{5}{2E_b} \left[ \sqrt{2} - \left( \frac{2\kappa^2}{\mu} E_b \right)^{1/4} \right]^2. \quad (7)$$

Figure 5 shows a comparison of screening lengths between the C2DB data and our results (using the BSE values  $E_b^{\text{BSE}}$  as the exciton binding energy). In most cases the absolute error between the present and the C2DB screening lengths is less than 5 Å (symbols within the gray region).

Alternatively, the screening length can be evaluated from the energy separations. Indeed, the expressions (3)–(5) lead to

$$r_0 \approx \frac{25}{8\beta E_b} \left( \sqrt{\frac{1}{2} + 2\sqrt{\frac{2}{5}}\beta} - \sqrt{\frac{1}{2}} \right)^4, \quad (8)$$

where  $\beta = \left( \frac{1}{1.175 \Delta_{12}} \right)^{25}$ . For a given screening length and average dielectric constant, the exciton reduced mass can also be estimated from the energy separations

$$\mu \approx \frac{\kappa^2}{r_0} \beta. \quad (9)$$

For instance, from the aforementioned RC measurements for a monolayer  $\text{WS}_2$  on a  $\text{SiO}_2/\text{Si}$  substrate [2], we obtain  $\kappa r_0 = 78.84$  Å ( $\kappa = 2$  [32],  $r_0 = 39.42$  Å) and  $\mu = 0.21$ . These results are comparable to the reported values [2]:  $\kappa r_0 = 75$  Å



and  $\mu = 0.16$ . The screening length and the exciton reduced mass for monolayer  $\text{WS}_2$  calculated from first principles are equal to 37.89 Å [29] and 0.15–0.22 [2], respectively.

In conclusion, we have derived analytical expressions (3) and (7) to theoretically calculate the exciton binding energy and the screening length, respectively. We have also introduced approximate expressions (6), (8), and (9) to experimentally determine the exciton binding energy (along with the quasiparticle band gap), the screening length, and the exciton reduced mass from measured exciton transition energies of the ground state (1s), and the first (2s) and the second (3s)

excited states. These expressions may be useful for studying 2D excitonic properties. In fact, knowledge of the exciton binding energy is necessary to understand the operation of optoelectronic devices based on 2D semiconductors, such as light-emitting diodes [37] and photovoltaic solar cells [38]. The determination of this quantity is also required to explain photoluminescence and electroluminescence measurements [39]. Besides the exciton binding energy, the screening length and the exciton reduced mass are also important quantities and are input to excitonic models [40]. Therefore, we expect the present results to be widely applicable.

- [1] G. D. Scholes and G. Rumbles, *Nat. Mater.* **5**, 683 (2006).
- [2] A. Chernikov, T. C. Berkelbach, H. M. Hill, A. Rigosi, Y. Li, O. B. Aslan, D. R. Reichman, M. S. Hybertsen, and T. F. Heinz, *Phys. Rev. Lett.* **113**, 076802 (2014).
- [3] K. He, N. Kumar, L. Zhao, Z. Wang, K. F. Mak, H. Zhao, and J. Shan, *Phys. Rev. Lett.* **113**, 026803 (2014).
- [4] M. M. Ugeda, A. J. Bradley, S.-F. Shi, F. H. da Jornada, Y. Zhang, D. Y. Qiu, W. Ruan, S.-K. Mo, Z. Hussain, Z.-X. Shen, F. Wang, S. G. Louie, and M. F. Crommie, *Nat. Mater.* **13**, 1091 (2014).
- [5] Z. Ye, T. Cao, K. O'Brien, H. Zhu, X. Yin, Y. Wang, S. G. Louie, and X. Zhang, *Nature (London)* **513**, 214 (2014).
- [6] H. M. Hill, A. F. Rigosi, C. Roquelet, A. Chernikov, T. C. Berkelbach, D. R. Reichman, M. S. Hybertsen, L. E. Brus, and T. F. Heinz, *Nano Lett.* **15**, 2992 (2015).
- [7] A. V. Stier, N. P. Wilson, K. A. Velizhanin, J. Kono, X. Xu, and S. A. Crooker, *Phys. Rev. Lett.* **120**, 057405 (2018).
- [8] M. Florian, M. Hartmann, A. Steinhoff, J. Klein, A. W. Holleitner, J. J. Finley, T. O. Wehling, M. Kaniber, and C. Gies, *Nano Lett.* **18**, 2725 (2018).
- [9] E. Lorchat, L. E. P. López, C. Robert, D. Lagarde, G. Froehlicher, T. Taniguchi, K. Watanabe, X. Marie, and S. Berciaud, *Nat. Nanotechnol.* **15**, 283 (2020).
- [10] G. H. Wannier, *Phys. Rev.* **52**, 191 (1937).
- [11] R. J. Elliott, *Phys. Rev.* **108**, 1384 (1957).
- [12] S. W. Koch, M. Kira, G. Khitrova, and H. M. Gibbs, *Nat. Mater.* **5**, 523 (2006).
- [13] X. L. Yang, S. H. Guo, F. T. Chan, K. W. Wong, and W. Y. Ching, *Phys. Rev. A* **43**, 1186 (1991).
- [14] T. Olsen, S. Latini, F. Rasmussen, and K. S. Thygesen, *Phys. Rev. Lett.* **116**, 056401 (2016).
- [15] A. V. Stier, N. P. Wilson, G. Clark, X. Xu, and S. A. Crooker, *Nano Lett.* **16**, 7054 (2016).
- [16] P. Cudazzo, I. V. Tokatly, and A. Rubio, *Phys. Rev. B* **84**, 085406 (2011).
- [17] N. S. Rytova, *Moscow Univ. Phys. Bull.* **22**, 18 (1967).
- [18] L. V. Keldysh, *J. Exp. Theor. Phys. Lett.* **29**, 658 (1979).
- [19] M. R. Molas, A. O. Slobodeniuk, K. Nogajewski, M. Bartos, Ł. Bala, A. Babiński, K. Watanabe, T. Taniguchi, C. Faugeras, and M. Potemski, *Phys. Rev. Lett.* **123**, 136801 (2019).
- [20] F. Gesztesy and L. Pittner, *J. Phys. A: Math. Gen.* **11**, 679 (1978).
- [21] H. J. W. Müller-Kirsten and S. K. Bose, *J. Math. Phys.* **20**, 2471 (1979).
- [22] T. Imbo, A. Pagnamenta, and U. Sukhatme, *Phys. Rev. D* **29**, 1669 (1984).
- [23] K. Eveker, D. Grow, B. Jost, C. E. Monfort, K. W. Nelson, C. Stroh, and R. C. Witt, *Am. J. Phys.* **58**, 1183 (1990).
- [24] See Supplemental Material at <http://link.aps.org/supplemental/10.1103/PhysRevB.105.L201407> for material parameters and the theoretical derivation.
- [25] S. Haastrup, M. Strange, M. Pandey, T. Deilmann, P. S. Schmidt, N. F. Hinsche, M. N. Gjerding, D. Torelli, P. M. Larsen, A. C. Riis-Jensen, J. Gath, K. W. Jacobsen, J. Jørgen Mortensen, T. Olsen, and K. S. Thygesen, *2D Mater.* **5**, 042002 (2018).
- [26] M. N. Gjerding, A. Taghizadeh, A. Rasmussen, S. Ali, F. Bertoldo, T. Deilmann, N. R. Knøsgaard, M. Kruse, A. H. Larsen, S. Manti, T. G. Pedersen, U. Petralanda, T. Skovhus, M. K. Svendsen, J. J. Mortensen, T. Olsen, and K. S. Thygesen, *2D Mater.* **8**, 044002 (2021).
- [27] A. F. Nikiforov and V. B. Uvarov, *Special Functions of Mathematical Physics* (Birkhäuser, Basel, 1988).
- [28] M. Pillai, J. Goglio, and T. G. Walker, *Am. J. Phys.* **80**, 1017 (2012).
- [29] M. Van der Donck, M. Zarenia, and F. M. Peeters, *Phys. Rev. B* **97**, 195408 (2018).
- [30] W.-T. Hsu, J. Quan, C.-Y. Wang, L.-S. Lu, M. Campbell, W.-H. Chang, L.-J. Li, X. Li, and C.-K. Shih, *2D Mater.* **6**, 025028 (2019).
- [31] E. Liu, J. van Baren, T. Taniguchi, K. Watanabe, Y.-C. Chang, and C. H. Lui, *Phys. Rev. B* **99**, 205420 (2019).
- [32] I. Kylänpää and H.-P. Komsa, *Phys. Rev. B* **92**, 205418 (2015).
- [33] T. C. Berkelbach, M. S. Hybertsen, and D. R. Reichman, *Phys. Rev. B* **88**, 045318 (2013).
- [34] D. W. Kidd, D. K. Zhang, and K. Varga, *Phys. Rev. B* **93**, 125423 (2016).
- [35] M. Z. Mayers, T. C. Berkelbach, M. S. Hybertsen, and D. R. Reichman, *Phys. Rev. B* **92**, 161404(R) (2015).
- [36] A. Raja, A. Chaves, J. Yu, G. Arefe, H. M. Hill, A. F. Rigosi, T. C. Berkelbach, P. Nagler, C. Schüller, T. Korn, C. Nuckolls, J. Hone, L. E. Brus, T. F. Heinz, D. R. Reichman, and A. Chernikov, *Nat. Commun.* **8**, 15251 (2017).
- [37] J. S. Ross, P. Klement, A. M. Jones, N. J. Ghimire, J. Yan, D. G. Mandrus, T. Taniguchi, K. Watanabe, K. Kitamura, W. Yao, D. H. Cobden, and X. Xu, *Nat. Nanotechnol.* **9**, 268 (2014).
- [38] A. Pospischil, M. M. Furchi, and T. Mueller, *Nat. Nanotechnol.* **9**, 257 (2014).
- [39] R. S. Sundaram, M. Engel, A. Lombardo, R. Krupke, A. C. Ferrari, P. Avouris, and M. Steiner, *Nano Lett.* **13**, 1416 (2013).
- [40] Y. Xu, C. Horn, J. Zhu, Y. Tang, L. Ma, L. Li, S. Liu, K. Watanabe, T. Taniguchi, J. C. Hone, J. Shan, and K. F. Mak, *Nat. Mater.* **20**, 645 (2021).